Demonstration of integrated polarization control with a 40 dB range in extinction ratio

Sarmiento-Merenguel, J. D.; Halir, R.; Le Roux, X.; Alonso-Ramos, C.; Vivien, L.; Cheben, P.; Durán-Valdeiglesias, E.; Molina-Fernández, I.; Marris-Morini, D.; Xu, D.-X.; Schmid, J. H.; Janz, S.; Ortega-Moñux, A.

Publisher's version / Version de l'éditeur:
https://doi.org/10.1364/OPTICA.2.001019
Optica, 2, 12, pp. 1019-1023, 2015-11-30

optica

Demonstration of integrated polarization control with a 40 dB range in extinction ratio

J. D. Sarmiento-Merenguel,[1,*] R. Halir,[1] X. Le Roux,[2] C. Alonso-Ramos,[2] L. Vivien,[2] P. Cheben,[3] E. Durán-Valdeiglesias,[2] I. Molina-Fernández,[1] D. Marris-Morini,[2] D.-X. Xu,[3] J. H. Schmid,[3] S. Janz,[3] and A. Ortega-Moñux[1]

[1]Departamento Ingeniería de Comunicaciones, ETSI Telecomunicación, Universidad de Málaga, 29071 Málaga, Spain
[2]Institut d'Electronique Fondamentale, Université Paris-Sud CNRS–UMR8622, Bat. 220, F-91405 Orsay, France
[3]National Research Council Canada, Ottawa, Ontario K1A 0R6, Canada
*Corresponding author: jdsm@ic.uma.es

Received 17 August 2015; revised 16 October 2015; accepted 17 October 2015 (Doc. ID 247924); published 30 November 2015

Polarization controllers are key elements in many fields of optics, including coherent communications, optical imaging, and quantum applications. Here we present a technology-independent polarization controller scheme based on electrically tunable phase shifters and polarization rotators with largely relaxed fabrication tolerances. Using this scheme, we experimentally demonstrate a fully integrated polarization controller in the silicon-on-insulator platform that is tunable over the complete C-band and achieves a polarization extinction range of 40 dB (±20 dB). These results constitute, to the best of our knowledge, the highest polarization extinction range achieved in a fully integrated device, and overcome the existing limitation in the trade-off between integration and performance in polarization management circuits.

OCIS codes: (130.3120) Integrated optics devices; (230.5440) Polarization-selective devices; (230.7370) Waveguides.

http://dx.doi.org/10.1364/OPTICA.2.001019

1. INTRODUCTION

Polarization management is of fundamental importance in many fields of photonics, including imaging [1], optical communications [2,3], and quantum information [4]. Compared to fiber or bulk optics solutions, integrated polarization handling holds potential for devices that are compact and low cost with, at the same time, improved stability. However, due to high sensitivity to fabrication imperfections, the integration of polarization managing elements is highly challenging. While promising advances have been recently made for polarization splitters [5,6], polarization control still requires a significant trade-off between the level of integration and performance. A polarization controller is composed of two main elements: polarization rotators (PRs) (or wave plates) with precisely controlled rotation angles and polarization phase shifters. While the latter can be implemented with judiciously designed waveguide heaters, the former require either specialized fabrication processes and materials [7,8] or extremely tight fabrication tolerances on the order of a few nanometers [9]. Indeed, the polarization controllers proposed in [10,11], which rely on precise PRs, have been experimentally demonstrated only with a hybrid integration approach. The devices presented in [12,13] are based on an alternative architecture but require high-performance polarization rotator-splitters. A further approach is based on quantum effects at a macroscopic scale, but it requires out-of-plane waveguides [14]. The maximum polarization extinction ratio (PER) that has been reported so far is ±10 dB (20 dB range) for fully integrated schemes and ±20 dB (40 dB range) for hybrid integration approaches.

Here we demonstrate, for what we believe is the first time, a fully integrated polarization controller that overcomes the trade-off between integration and performance. Our design yields a PER range of ∼40 dB, which is, furthermore, tunable in the full C-band. This is achieved by using three polarization-rotating elements, as first proposed for PRs in [9], combined with polarization phase shifters. The key advantage of our scheme is that the polarization phase shifters both compensate fabrication deviations in the PRs and enable wavelength tuning over a range of at least 40 nm.

2. DEVICE OPERATION

The structure that we propose is shown in Fig. 1. In order to describe its operation it is convenient to recall the following polarization concepts: a polarized lightwave is generally described using the Jones vector $\tilde{J} = [E_x e^{j\varphi_x}; E_y e^{j\varphi_y}]$, where $E_{x,y}$ and $\varphi_{x,y}$ are the amplitude and phase of the electric field components in the horizontal (x) and vertical (y) directions. For the purpose of our discussion, the state of polarization (SOP) of the wave is defined with two parameters: the PER and the polarization phase (ρ). The PER is defined as the ratio of power in the vertical and horizontal component, $\mathrm{PER} = |E_y|^2/|E_x|^2$, so that a horizontally polarized

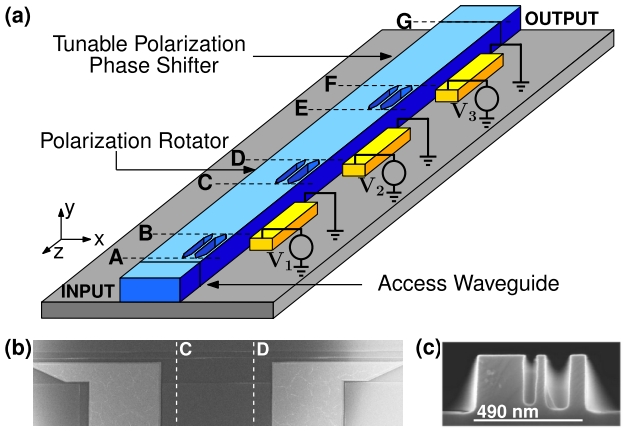

Fig. 1. (a) The proposed polarization controller consists of three PRs (etched waveguide sections) and three tunable polarization phase shifters (implemented here with waveguide heaters). Even with highly imperfect PRs, complete polarization control is feasible. (b) Scanning electron microscope image of waveguide and heater pads (top view) and (c) the PRs (cross section).

wave has PER = 0, and a vertically polarized wave has PER = ∞. The polarization phase, ρ, is defined as the phase difference between the components, $\rho = \varphi_y - \varphi_x$. As an example, right-handed circular polarization corresponds to PER = 1 and $\rho = 90°$.

Our integrated polarization controller, shown in Fig. 1, controls the SOP using two types of elements: PRs, which mainly change the PER and, to some extent, the polarization phase, ρ; and tunable polarization phase shifters (TPPSs) that control the polarization phase, ρ, without altering the PER.

The operation of the device is illustrated in the Poincaré sphere in Fig. 2. Let us consider horizontally polarized light at the input (point A) and right-handed circular polarization as the desired output SOP (point G). First, a certain polarization rotation will

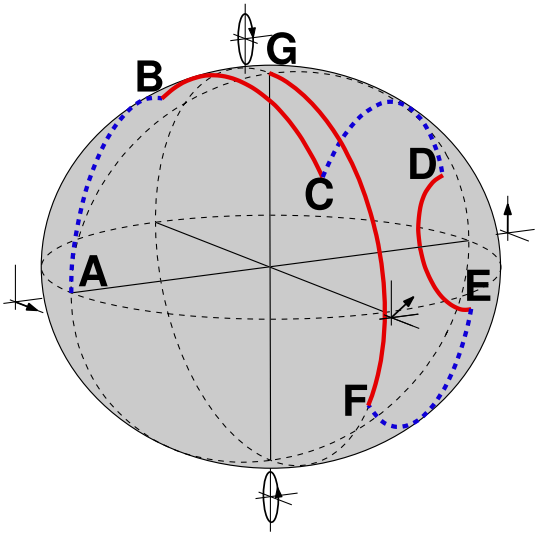

Fig. 2. Evolution of state of polarization throughout the device. The input state of polarization is horizontal (point A), and the output state of polarization is right-handed circular (point G). The blue dotted lines correspond to PRs, whereas red lines correspond to tunable polarization phase shifters. The points named A through G correspond with the planes A through G in Fig. 1.

be performed in the first PR (point B). Following the first PR there are two pairs of TPPS–PR. Each TPPS will tune the polarization phase in order to feed the PRs with the suitable polarization phase so that, at the output of the third PR (point F), the desired PER is achieved. The last TPPS then produces the appropriate polarization phase shift so that the desired SOP is obtained at the output (point G) [9,15].

PRs can be implemented using various mechanisms, such as modal evolution [13], cross-polarization coupling [16] and rotator waveguides [17]. One of the key advantages of our scheme compared to previously proposed devices [10] is that the individual PRs do not need to produce a specific polarization conversion. Instead, given horizontal input polarization, they must only produce at their output a SOP with PER in the range [15]

$$-4.7 \text{ dB} < \text{PER} < 4.7 \text{ dB}. \quad (1)$$

Given a nominal design of a PR, the above condition is fulfilled in a wide range of fabrication deviations, making this scheme highly tolerant to fabrication errors. Tunable polarization phase shifters are required to provide polarization phase shifts in the range $[0–2\pi]$.

3. DEVICE IMPLEMENTATION

A. Design

To experimentally demonstrate our approach, a silicon-on-insulator proof-of-concept device has been fabricated. The nominal dimensions of the waveguide core are 490 nm × 260 nm and the device is clad with a SU-8 polymer layer, resulting in a waveguide birefringence of $n_{\text{eff}}^{\text{TE}} - n_{\text{eff}}^{\text{TM}} = 0.45$. The PR has been implemented following the approach described in [17], where vertical symmetry is broken by forming two subwavelength trenches; see Fig. 1(c). The trenches are ∼60 and ∼100 nm wide, separated by a ∼40 nm silicon slice, and placed ∼60 nm from the waveguide sidewall. Trench depths are determined by the etch-lag effect, being ∼230 and ∼250 nm deep, respectively. The length of the rotator is 20 μm. It has to be noted that the exact dimensions are not crucial for the operation of the device, provided that the PRs exhibit a PER in the range defined by Eq. (1).

To realize the TPPS, we take advantage of the opposite thermo-optic coefficients of silicon dioxide, $dn_{\text{SiO}_2}/dT = 1 \times 10^{-5}\text{°C}^{-1}$ and SU-8 $dn_{\text{SU-8}}/dT = -1.1 \times 10^{-4}\text{°C}^{-1}$; the thermo-optic coefficient of silicon is $dn_{\text{Si}}/dT = 1.8 \times 10^{-4}\text{°C}^{-1}$ [18]. By including these thermo-optic coefficients in a mode solver to account for the polarization-dependent modal confinement, the effective thermo-optic coefficients for horizontal and vertical polarization are obtained: $dn_{\text{eff}}^{\text{TE}}/dT = 1.7 \times 10^{-4}\text{°C}^{-1}$ and $dn_{\text{eff}}^{\text{TM}}/dT = 1.1 \times 10^{-4}\text{°C}^{-1}$. The polarization phase shift ρ induced by a temperature variation ΔT in the TPPS waveguide is then given by

$$\rho = 2\pi \frac{L_{\text{TPPS}}}{\lambda} \left[\left(n_{\text{eff}}^{\text{TE}} - n_{\text{eff}}^{\text{TM}} \right) + \Delta T \left(\frac{dn_{\text{eff}}^{\text{TE}}}{dT} - \frac{dn_{\text{eff}}^{\text{TM}}}{dT} \right) \right]. \quad (2)$$

The design of the length of the phase shifter, L_{TPPS}, requires a trade-off between bandwidth and maximum temperature increase. Shorter lengths require higher temperature increments in order to achieve a full 2π variation in ρ, as shown in Fig. 3. On the other hand, large values of L_{TPPS} result in a strong wavelength dependence of ρ, which ultimately limits the operational bandwidth of the polarization controller. This bandwidth can

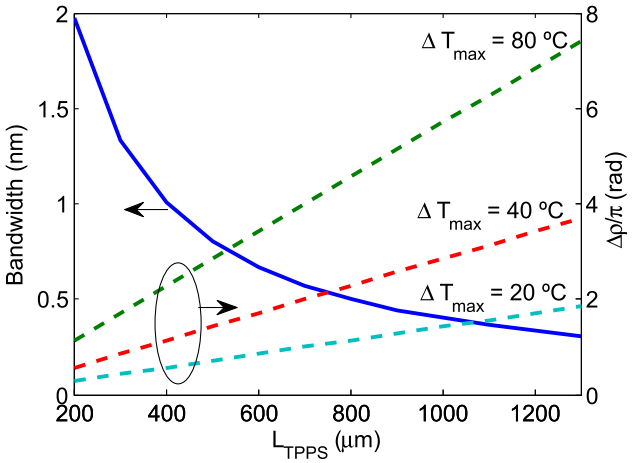

Fig. 3. Dashed lines: polarization phase shift, $\Delta\rho$, of a single TPPS as a function of its length for different maximum temperature increases, ΔT_{max}, obtained from Eq. (2). Solid line: estimated bandwidth of the complete polarization controller as a function of the length of the TPPS.

be estimated numerically, by modeling the device as a concatenation of Jones matrices, resulting in the plot shown in Fig. 3. Bandwidth is defined as the wavelength range in which the PER is larger than 16 dB. From Fig. 3, the minimum length that achieves a 2π variation of ρ with a moderate temperature increase of 40°C is $L_{TPPS} = 700$ μm, with a bandwidth of ∼0.6 nm. In this proof-on-concept design, bandwidth was not deemed as critical as achieving the full phase swing, so the TPPS length was overdimensioned to 1000 μm, yielding an estimated bandwidth of ∼0.4 nm.

The TPPS was implemented through waveguide heaters placed alongside the waveguide, as shown in Figs. 1(a) and 1(b). Waveguide heaters are 2 μm wide chromium–gold electrodes spaced 2 μm from the waveguide to avoid losses due to interaction of the evanescent waveguide field with the metallization. Simulations show that for a 1 μm spacing, losses are still negligible, so that the efficiency of the heaters could be further increased by reducing this spacing.

Together with the complete polarization controller, test structures of its individual components (straight waveguides, PRs, and polarization phase shifters) were included on the same chip.

B. Fabrication

The photonic structures and isolation regions for metallic contacts were defined with ZEP electron beam (e-beam) positive resist lithography, and transferred to the silicon layer with inductively coupled plasma etching. A single, full etch step was used, leveraging the etch-lag effect to define the partially etched slots in PRs [see Fig. 1(c)]. The waveguide heaters were realized with 100-nm-thick chromium–gold electrodes fabricated with e-beam evaporation and a lift-off process; they had a measured resistance of ∼165Ω. Finally, waveguides were selectively covered with a UV lithography patterned 5 μm thick SU-8 negative resist, facilitating access to the metallic pads. Once thermally cross linked, SU-8 is thermally stable beyond 200°C.

C. Experimental Results

For the characterization of the device, horizontally polarized light from a tunable laser was coupled into the waveguide with a polarization-maintaining lensed fiber. At the output of the chip, light was collected by a microscope objective and then filtered by a linear polarizer, positioned on a rotary mount. Depending on the rotation of the polarizer, only horizontally or vertically polarized light is transmitted to the detector, which consisted of an infrared camera. The setup was calibrated using the reference straight waveguides, yielding a maximum measurable PER of ∼25 dB. In order to tune the polarization controller, DC currents are injected in the two first TPPSs, locally heating the waveguide and thus changing the PER of the output SOP.

In a first experiment, we verified that a single TPPS was able to cover a full 2π polarization phase shift. Light polarized at 45° was injected in a test structure with no PRs and a single active tunable polarization phase shifter, exciting both the horizontally (quasi-TE) and vertically (quasi-TM) polarized waveguides modes. Upon heating the TPPS, the phase shift ($\Delta\rho$) between the horizontal and vertical polarization component changes, resulting in a polarization state that periodically progresses from linear at +45°, to right-handed circular, to linear at −45°, and left-handed circular. Passing the resulting output light through a linear polarizer at +45° and detecting the optical power then yields the sinusoidal signal $(1 + \cos\ \Delta\rho)$, from which the polarization phase $\Delta\rho$ shift is obtained. As increasing power was applied to the TPPS, we observed several cycles of this signal, extracting a tuning efficiency of ∼70 rad/W.

In a second experiment, using the full polarization controller [see Fig. 1(a)] with horizontally polarized light at the input, we generated vertical output polarization achieving a PER of +20 dB ($|E_y|^2/|E_x|^2 = 100$) and horizontal output polarization achieving a PER of −20 dB ($|E_y|^2/|E_x|^2 = 0.01$) at $\lambda = 1.55$ μm. The tuning algorithm relies on minimizing the power in the SOP orthogonal to the desired one. This is achieved by varying the voltage in one of the TPPSs. Once a minimum is found, the other TPPS is tuned. A few iterations of these steps suffice to optimize the desired PER.

Insertion losses of the polarization controller, excluding fiber-to-chip coupling, were found to be below 3 dB. The main contribution of the losses comes from the PR, with individual insertion losses of ∼0.7 dB [17]. The total electrical power required for tuning was on average ∼300 mW, with a peak value of ∼700 mW. The bandwidth of the device is ∼0.5 nm and is limited by the TPPSs, as explained before. This limitation is, however, not intrinsic to the polarization controller scheme and can be overcome using, for instance, a TPPS based on nematic liquid crystals, which exhibit an electrically tunable anisotropy [19]. This could reduce its length below 200 μm, yielding a bandwidth in excess of 2 nm.

To show that any intermediate PER can be generated, we developed the third experiment. Let $(\rho_{1,y}, \rho_{2,y})$ and $(\rho_{1,x}, \rho_{2,x})$ be the phase shift set on the first and second TPPSs to obtain vertical and horizontal polarization at the output, respectively [see Fig. 4(a)]. To generate intermediate values of PER, the phase shift is linearly swept between these pairs, by means of the applied voltages V_1 and V_2. We start with vertical polarization at the output with phase shifts $(\rho_{1,y}, \rho_{2,y})$. We then increase ρ_1, until $\rho_{1,x}$ is reached. ρ_2 is then swept in the same way, obtaining horizontal polarization at the end of the process. Intermediate values of ρ_1 and ρ_2 should produce intermediate values of PER. Figure 4 shows the results of this experiment in terms of polarization phase shifts ρ_1

and ρ_2. Figure 4(a) represents the simulated PER as a function of ρ_1 and ρ_2. The path corresponding to the specific combinations of (ρ_1, ρ_2) is superimposed: the solid line corresponds to variations of ρ_1, and the dashed line corresponds to variations of ρ_2. Figure 4(b) compares the measured and simulated PER along that path, in terms of the phase variations $\Delta\rho_{1,2}$. A good agreement between the simulated and experimental results is achieved, confirming that the device indeed can generate any PER at its output. From this experiment, we found the tuning rate of the TPPSs to be ~20 rad/W. The difference with the tuning efficiency derived from the first experiment is attributed to thermal crosstalk between the heaters.

To prove that the device also gives control over the polarization phase (ρ), we carried out the fourth experiment. In this case, a voltage was applied to the third heater (V_3); ideally, this should produce a constant PER, while varying ρ over a full 2π range. To measure the resulting polarization state, we recorded the power (p) passing through the polarizer rotated at –45°, 0°, +45°, 90°, corresponding to the polarization states: linear at –45°, horizontal, linear at +45°, and vertical. From these measurements the normalized Stokes parameters s_1 and s_2 are computed as $s_1 = (p_{0°} - p_{90°})/(p_{0°} + p_{90°})$ and $s_2 = (p_{+45°} - p_{-45°})/(p_{+45°} + p_{-45°})$. The resulting pairs ($s_1$, s_2) are shown as the green trace in Fig. 5. To appreciate the effect more clearly, we project the pairs (s_1, s_2) on the surface of the sphere, by calculating the third Stokes parameter as $s_3 = \pm[1 - (s_1^2 + s_2^2)]^{1/2}$ (this can be done because we are working with fully polarized light, so that $s_1^2 + s_2^2 + s_3^2 = 1$). The resulting blue trace in Fig. 5 reveals that, as expected, the PER does not change significantly, but the polarization phase ρ varies over a full 2π range. Together with the previous experiment showing full control over the PER, this demonstrates that the device can indeed fully control the polarization state. We estimate the degree of coverage of the Poincaré sphere of this device to be 98%, limited only by the measured PER (±20 dB)

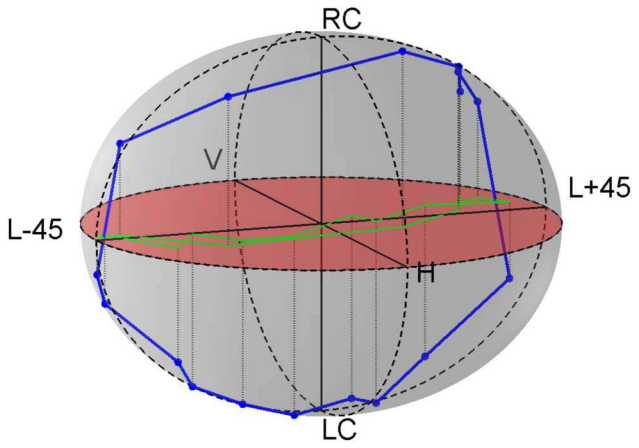

Fig. 5. Measured polarization state as an increasing voltage is applied at the third heater (V_3), showing that any polarization phase (ρ) can be generated. The blue trace is obtained from the measured data points (green trace) by projection on the surface of the Poincaré sphere.

A final experiment showing that the device can operate in a wide wavelength range was performed. Figure 6 shows the PER of the device in the C-band. Note that the measured PER of the individual PR fluctuates in a range of ~3 dB, confirming that, as predicted by condition (1), full polarization control is possible even with variable rotator performance. Indeed, the complete polarization controller can be tuned to extinction ratios better than ±20 dB. The measured PER range is ~40 dB in the full C-band, yielding an unprecedented enhancement of 2 orders

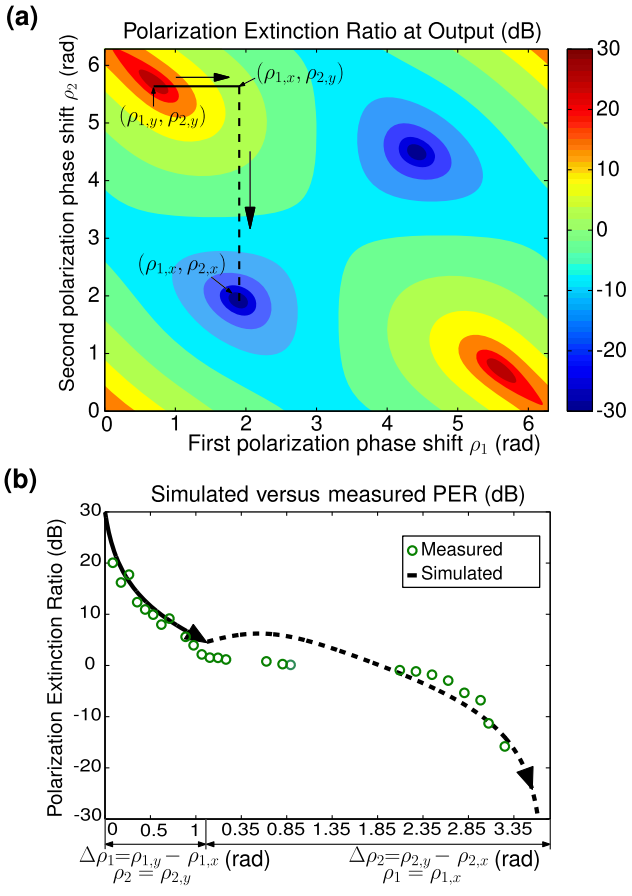

Fig. 4. (a) Simulated PER at the output of the polarization controller as a function of the phase shifts introduced in the two first TPPSs, when horizontally polarized light is launched into the device at $\lambda = 1.55$ μm. (b) Measured PER compared to the simulated PER corresponding to the path shown in (a). There was no measurable variation of PER in the $\Delta\rho_2 \approx [0.85–2.3]$ range.

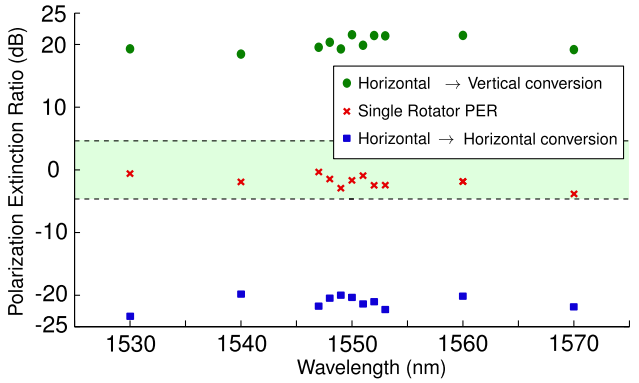

Fig. 6. Measured PER when horizontally polarized light is launched into the device. Tuning of the integrated polarization controller provides a PER range of ~40 dB at any C-band wavelength, even with individual rotators that exhibit a variable PER. The shaded area corresponds to condition (1).

of magnitude compared to other state-of-the-art integrated polarization controllers.

4. CONCLUSIONS

In summary, a fully integrated polarization controller scheme was experimentally demonstrated. To the best of our knowledge, this is the first fully integrated polarization controller achieving an ~40 dB polarization extinction range, tunable in the full C-band. Our scheme enables not only wavelength tuning, but also compensation of fabrication deviations, for any photonic platform. We believe that this work opens the path toward reliable monolithic integration of polarization controllers, with many potential applications, including polarization optical circuits, imaging, and quantum communications, to name a few.

Funding. Fondo Europeo de Desarrollo Regional—FEDER; French RENATECH network; Institut Universitaire de France; Ministerio de Economía y Competitividad (TEC2013-46917-C2-1-R).

Acknowledgment. The fabrication of the device was performed at the nano-center CTU-IEF-Minerve, which is partially funded by the Conseil Général de l'Essonne. D.M.-M. acknowledges support by the Institut Universitaire de France.

REFERENCES

1. R. S. Gurjar, V. Backman, L. T. Perelman, I. Georgakoudi, K. Badizadegan, I. Itzkan, R. R. Dasari, and M. S. Feld, "Imaging human epithelial properties with polarized light-scattering spectroscopy," Nat. Med. **7**, 1245–1248 (2001).
2. E. Ip, A. P. T. Lau, D. J. Barros, and J. M. Kahn, "Coherent detection in optical fiber systems," Opt. Express **16**, 753–791 (2008).
3. H. Mardoyan, O. B. Pardo, P. Jennevé, G. de Valicourt, M. A. Mestre, S. Bigo, C. Kazmierski, N. Chimot, A. Steffan, J. Honecker, R. Zhang, P. Runge, A. Richter, C. Arellano, A. Ortega-Moñux, and I. Molina-Fernandez, "Pic-to-pic experiment at 130 Gb/s based on a monolithic transmitter using switching of prefixed optical phases and a monolithic coherent receiver," in *Optical Fiber Communication Conference: Postdeadline Papers* (2014), paper Th5C.2.
4. X.-S. Ma, T. Herbst, T. Scheidl, D. Wang, S. Kropatschek, W. Naylor, B. Wittmann, A. Mech, J. Kofler, E. Anisimova, V. Makarov, T. Jennewein, R. Ursin, and A. Zeilinger, "Quantum teleportation over 143 kilometres using active feed-forward," Nature **489**, 269–273 (2012).
5. D. Perez-Galacho, R. Zhang, A. Ortega-Moñux, R. Halir, C. Alonso-Ramos, P. Runge, K. Janiak, G. Zhou, H.-G. Bach, A. Steffan, and I. Molina-Fernandez, "Integrated polarization beam splitter for 100/400 GE polarization multiplexed coherent optical communications," J. Lightwave Technol. **32**, 361–368 (2014).
6. B. Shen, P. Wang, R. Polson, and R. Menon, "An integrated-nanophotonics polarization beamsplitter with 2.4 × 2.5 μm^2 footprint," Nat. Photonics **9**, 378–382 (2015).
7. G. Corrielli, A. Crespi, R. Geremia, R. Ramponi, L. Sansoni, A. Santinelli, P. Mataloni, F. Sciarrino, and R. Osellame, "Rotated waveplates in integrated waveguide optics," Nat. Commun. **5**, 4249 (2014).
8. C. Vicente, P. Lima, V. de Zea Bermudez, L. Carlos, P. Andre, and R. Ferreira, "Polarization state control using thermo-optic effect in organic-inorganic hybrid waveguides," in *16th International Conference on Transparent Optical Networks (ICTON)* (IEEE, 2014).
9. C. Alonso-Ramos, R. Halir, A. Ortega-Moñux, P. Cheben, L. Vivien, Í. Molina-Fernández, D. Marris-Morini, S. Janz, D.-X. Xu, and J. Schmid, "Highly tolerant tunable waveguide polarization rotator scheme," Opt. Lett. **37**, 3534–3536 (2012).
10. D. C. Hutchings and B. M. Holmes, "A waveguide polarization toolset design based on mode beating," IEEE Photon. J. **3**, 450–461 (2011).
11. J.-W. Kim, S.-H. Park, W.-S. Chu, and M.-C. Oh, "Integrated-optic polarization controllers incorporating polymer waveguide birefringence modulators," Opt. Express **20**, 12443–12448 (2012).
12. L. Moller, "WDM polarization controller in PLC technology," IEEE Photon. Technol. Lett. **13**, 585–587 (2001).
13. W. D. Sacher, Y. Huang, L. Ding, T. Barwicz, J. C. Mikkelsen, B. J. Taylor, G.-Q. Lo, and J. K. Poon, "Polarization rotator-splitters and controllers in a Si_3N_4-on-SOI integrated photonics platform," Opt. Express **22**, 11167–11174 (2014).
14. Q. Xu, L. Chen, M. G. Wood, P. Sun, and R. M. Reano, "Electrically tunable optical polarization rotation on a silicon chip using Berry's phase," Nat. Commun. **5**, 5337 (2014).
15. J. Sarmiento-Merenguel, C. Alonso-Ramos, R. Halir, L. Vivien, P. Cheben, A. Ortega-Moñux, I. Molina-Fernández, X. Leroux, D. Marris-Morini, D.-X. Xu, J. Schmid, and S. Janz, "Silicon-on-insulator polarization controller with relaxed fabrication tolerances," in *11th International Conference on Group IV Photonics* (IEEE, 2014), pp. 87–88.
16. D. Dai and J. E. Bowers, "Novel concept for ultracompact polarization splitter-rotator based on silicon nanowires," Opt. Express **19**, 10940–10949 (2011).
17. A. V. Velasco, M. L. Calvo, P. Cheben, A. Ortega-Moñux, J. H. Schmid, C. Alonso-Ramos, Í. Molina-Fernandez, J. Lapointe, M. Vachon, S. Janz, and D.-X. Xu, "Ultracompact polarization converter with a dual subwavelength trench built in a silicon-on-insulator waveguide," Opt. Lett. **37**, 365–367 (2012).
18. M. Ibrahim, J. H. Schmid, A. Aleali, P. Cheben, J. Lapointe, S. Janz, P. J. Bock, A. Densmore, B. Lamontagne, R. Ma, D.-X. Xu, and W. N. Ye, "Athermal silicon waveguides with bridged subwavelength gratings for TE and TM polarizations," Opt. Express **20**, 18356–18361 (2012).
19. J. Beeckman, R. James, F. Aníbal-Fernández, W. De-Cort, P. Vanbrabant, and K. Neyts, "Calculation of fully anisotropic liquid crystal waveguide modes," J. Lightwave Technol. **27**, 3812–3819 (2009).